# Simulation of passive myocardium of rabbit ventricles, using selective smoothed finite element method(S-FEM)

**C. Jiang[1], Zhi-Qian Zhang[2], *X. Han[1], G.R. Liu[3]**

[1] State Key Laboratory of Advanced Technology of Design and Manufacturing for Vehicle Body, Hunan University, P.R. China, 410082
[2] Institute of High Performance Computing, A*STAR, Singapore, 138632
[3] Department of Aerospace Engineering and Engineering Mechanics, University of Cincinnati, 2851 Woodside Dr, Cincinnati, OH 45221, USA

*Corresponding author: hanxu@hnu.edu.cn

## Abstract

A selective smoothed finite element method (Selective S-FEM) is developed for dynamic 3D analysis of extremely large deformation of incompressible bio-tissues, using the simplest 4-node tetrahedron elements. In the present selective S-FEM, face-based Smoothed FEM (FS-FEM) and node-based Smoothed FEM (NS-FEM) are, respectively, used for the deviatoric and volumetric parts of the deformation of incompressible bio-tissues. Therefore the "overly-soft" feature of the NS-FEM is made use of for mitigating the volumetric locking that may occur in bio soft tissue. Because the FS-FEM can provide close-to-exact stiffness, our selective S-FEM can provide an accurate solution. In the current formulation, the soft tissue is modeled using the hyperelastic constitutive law. Numerical examples are presented to simulate a passive filling process of anatomical rabbit ventricles. It is demonstrated that the Selective S-FEM possess good potential for accurately simulating the behavior of bio-tissues for reliable solution..

**Keywords:** Finite Element Method, Smoothed Finite Element Method, Gradient Smoothing, Incompressibility, Anisotropy, Myocardium, Tetrahedral, Large Deformation, Explicit time integration

## Introduction

The explicit dynamic Finite Element Method (FEM) has been successfully applied to solve transient nonlinear responses of various material and structural systems with large deformation and strain, impact-contact and metal forming problems in automotive, aerospace, and bioengineering (Goudreau and Hallquist 1982; Belytschko, Liu, and Moran 2000; Miller et al. 2006). In explicit dynamics analyses using FEM, four-node quadrilateral element (Q4) and eight-node hexahedron element (H8) are the most frequently used with single quadrature point for efficiency, which requires a hourglass control to remedy hourglass instability (spurious zero-energy modes) (Belytschko, Liu, and Moran 2000). In addition, the one-point quadrature technique can also mitigate the volumetric locking in nearly incompressible solids.

When quadrilateral and hexahedral elements are used, it is laborious and time-consuming in pre-processing and the remeshing for distorted elements, because of the difficulties in automatically meshing with these types of elements It is much easier to automatically create and refine, when using Triangular and Tetrahedral mesh (T-mesh) are used in complicated geometry. In fact, there are now many commercial and open-source softwares, have been developed for automotive generating T-meshes. However, in the FEM based on the standard weak formulation, the performance of T-mesh is usually very poor for its overly stiff behavior. This is in particular true for incompressible solids where volumetric locking may occur.

Many efforts have been made to enhance the capability of T-mesh in handling the incompressibility, including the F-bar method (De Souza Neto et al. 1996), the method using hydrostatic pressure as an additional independent variable (Zienkiewicz et al. 1998), nodal pressure average treatment (Bonet and Burton 1998), Hu-Washizu three fields variational theorem (Taylor 2000), and nodal averaging treatment of deformation gradient tensor (Bonet, Marriott, and Hassan 2001). The node-based strain smoothing has also been successfully applied to meshfree methods for stabilization (Chen, Yoon, and Wu 2002).

Models using smoothed strains can have a theoretical foundation on G space theory (Liu and Zhang 2009; Liu 2009; Liu and Zhang 2013). Because the G space theory allows the use of discontinuous functions, such a formulation is also termed as weakened weak (or W2) forms. Typical W2 formulation method is the Smoothed Point Interpolation Methods (S-PIM) (Liu and Zhang 2013). When functions in a FEM space are used in a W2 formulation, the so-called the smoothed finite element method or S-FEM. In terms of the way to construct the smoothing domains, S-FEM can have a family of methods of unique properties, which can be classified as cell-based smoothed FEM (CS-FEM) (Liu, Dai, and Nguyen 2006), node-based smoothed FEM (NS-FEM) (Nguyen-Thoi et al. 2010), edge-based S-FEM (ES-FEM) (Liu, Nguyen-Thoi, and Lam 2009) for 2D problems, and face-based S-FEM (FS-FEM) for 3D problems (Nguyen-Thoi et al. 2009). In these S-FEM methods, the NS-FEM has an unique property of volumetric locking free, due to its strong softening effects. However, spurious non-zero-energy eigen-modes and temporal instabilities arise for NS-FEM, despite the fact that it is proven spatially stable (Liu 2009; Liu, Dai, and Nguyen 2006). Differing from NS-FEM, the ES-FEM or FS-FEM that uses edge-based or face-based smoothing domains are found both spatial and temporal stable, because of using more smooth domains. However, ES-FEM or FS-FEM usually produces slightly overestimated stiffness, and hence it can also suffer from the volumetric locking. A method using selective gradient-smoothing technique, so called Selective S-FEM, has been proposed in order to eliminate volumetric locking, at the same time, improve the performance of the simplex TRI3 and TET4 elements. The employment of the combined edge-based and node-based smoothing operations enables effective handling of element distortion in extremely large deformation with low computation cost.

Biological tissues, like skin, myocardium, arterial layer, can often treated as hyperelastic material. This is because they can undergo very large deformation, and after unloading, they can recover to original state. These strain energy functions can be divided into two groups by their variables. The first group is the strain-based strain energy functions, such as the Fung form for arterial layer (Chuong and Fung 1986) and the McCulloch exponential form for myocardium (Vetter and McCulloch 2000), which regard strains as independent variables. The another group is the invariant-based strain energy functions, like the Hozapfel-Gasser-Odgen form for arterial layer (Gasser, Ogden, and Holzapfel 2006) , the Lin form (Lin and Yin 1998) for rabbit heart, and the Ogden form (Ogden 1972) for extremely large deformation.

In this paper, we first introduce the basic formulations of explicit dynamic nonlinear Selective S-FEM in Section 1, and then briefly review the strain energy functions of bio-tissues in Section 2. Following numerical examples of transversely isotropic hyperelastic plate and passive bi-ventricles in Section 3, conclusions are drawn in Section 4.

**Explicit Dynamic nonlinear Selective S-FEM**

In dynamic analysis, inertia and damping effects must be considered, and the discrete form of the governing equation can be given in general as follow

$$\boldsymbol{M}\ddot{\boldsymbol{u}}+\boldsymbol{C}\dot{\boldsymbol{u}}+\boldsymbol{F}_{\text{int}}=\boldsymbol{F}_{\text{ext}} \tag{1}$$

where $\boldsymbol{u}$ is nodal displacements vector, and $\boldsymbol{M}=\int_{\Omega}\boldsymbol{N}^{\mathrm{T}}\boldsymbol{\rho}\boldsymbol{N}d\Omega$ ( $\boldsymbol{\rho}$ is mass density vector), $\boldsymbol{C}=\int_{\Omega}\boldsymbol{N}^{\mathrm{T}}\boldsymbol{c}\boldsymbol{N}d\Omega$ ( $\boldsymbol{c}$ is damping coefficient vector), $\boldsymbol{F}_{\text{ext}}=\int_{\Omega}\boldsymbol{N}^{\mathrm{T}}\boldsymbol{b}d\Omega+\int_{\Gamma_{\mathrm{t}}}\boldsymbol{N}^{\mathrm{T}}\boldsymbol{t}d\Gamma_{\mathrm{t}}$.

In general S-FEM, nodal internal forces should be computed from smoothed strain matrix and smoothed stress,

$$\boldsymbol{F}_{\text{int}}=\int_{\Omega}\tilde{\boldsymbol{B}}^{T}\tilde{\boldsymbol{\sigma}}d\Omega \tag{2}$$

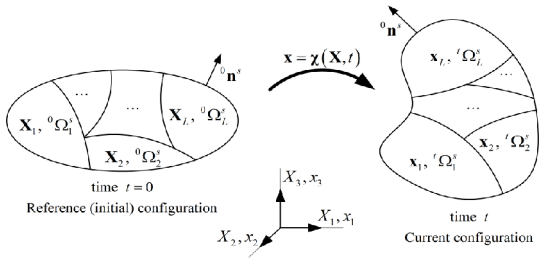


Figure 1. Configuration and motion of a continuum body, and smoothing domains

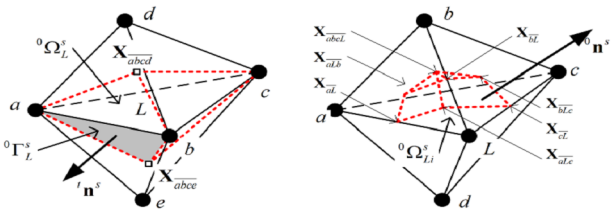

Figure 2. Illustrations of smoothing domains of (left) FS-FEM-TET4 (right) NS-FEM-TET4

In this paper, total Lagrange formulation is employed to solve geometrical nonlinearity. The initial reference configuration of material point in a body $\Omega$ is denoted by $\boldsymbol{X}$, and displacement at time $t_n$ is denoted as $\boldsymbol{u}_n$ then the current deformed configuration is expressed as

$$\boldsymbol{x}_n=\boldsymbol{X}+\boldsymbol{u}_n \tag{3}$$

There is the deformation gradient tensor of $\boldsymbol{X}$ which is the measure of deformation from reference configuration, as in Figure 1. It is given by

$$\boldsymbol{F}_{\mathrm{n}}=\frac{\partial \boldsymbol{x}_{\mathrm{n}}}{\partial \boldsymbol{X}} \tag{4}$$

In our S-FEM, the deformation gradient tensor needs also be written in smoothed version, as below

$$\tilde{F}_{ij}=\frac{1}{{}^{0}A_{L}^{s}}\int_{{}^{0}\Omega_{L}^{s}}\tilde{F}_{ij}\left(\boldsymbol{X}_{L}\right)d\Omega=\frac{1}{{}^{0}A_{L}^{s}}\int_{{}^{0}\Gamma_{L}^{s}}u_{i}\,{}^{0}n_{j}^{s}d\Gamma+\delta_{ij}=\tilde{\mathrm{e}}_{ij}\left(\boldsymbol{X}_{L}\right)+\delta_{ij}, \tag{5}$$

where ${}^{0}A_{L}^{s}$ is the area of initial smooth domains.

For hyperelastic incompressible biology material, the corresponding strain energy function is often split into volumetric part and deviatoric part. The smoothed second Piola-Kirchoff (PK2) stress tensor can be calculated by given strain energy function and smoothed deformation gradient as follows

$$\tilde{S}_{ij}=\frac{\partial\Psi}{\partial\tilde{E}_{ij}}=2\frac{\partial\Psi}{\partial\tilde{C}_{ij}}=2\frac{\partial\Psi^{\text{vol}}}{\partial\tilde{C}_{ij}^{\text{NS-FEM}}}+2\frac{\partial\Psi^{\text{dev}}}{\partial\tilde{C}_{ij}^{\text{FS-FEM}}} \tag{6}$$

where $\tilde{E}_{ij}$ is the *Green strain tensor*, the smoothed *right Cauchy-Green strain tensor* $\tilde{C}_{ij}=\tilde{F}_{ki}\tilde{F}_{kj}$. After getting the PK2 stress tensor, substitute it into Eq.(2) to get internal nodal force vector.

In the Selective S-FEM, its strain smoothing is performed using a combination of edge-based smoothing in 2D problem (face-based smoothing in 3D) and node-based smoothing. These two types of smooth domains in Selective S-FEM used here are plotted in Figure 2. In Selective S-FEM, volumetric part of PK2 stress is computed by the "over-softly" NS-FEM, and the deviatoric part of

PK2 stress is handled by more precise ES-FEM using smoothed deformation gradient tensor from Eq.(5).

For the time integration, the well-established explicit central differential method is used. Although explicit scheme is conditional stable, it is much easier in programming and no need to form the global tangent stiffness matrix. The time increments are defined as

$$\Delta t^{n+1/2} = t^{n+1} - t^n,\ t^{n+1/2} = \left(t^{n+1} + t^n\right)/2,\ \Delta t^n = t^{n+1/2} - t^{n-1/2}. \tag{7}$$

The displacement and velocity can be update by

$$\boldsymbol{u}^n = \boldsymbol{u}^{n+1} + \boldsymbol{v}^{n+1/2}\Delta t^{n+1/2}, \tag{8}$$

$$\boldsymbol{v}^{n+1/2} = \boldsymbol{v}^{n-1/2} + \Delta t^n \boldsymbol{a}^n, \tag{9}$$

The acceleration $\boldsymbol{a}^n = \ddot{\boldsymbol{u}}^n$ is obtained by solving the following equation

$$\boldsymbol{M}\boldsymbol{a}^n = \boldsymbol{f}^{ext}\left(\boldsymbol{u}^n, t^n\right) - \overline{\boldsymbol{f}}^{int}\left(\boldsymbol{u}^n, t^n\right) - \boldsymbol{C}\boldsymbol{v}^n. \tag{10}$$

If a lumped mass matrix is employed in Eq.(10), $\boldsymbol{M}$ becomes a diagonal matrix, and $\boldsymbol{a}^n$ can be computed via trivial operations without invoking a linear algebra equation solver.

**Hyperelastic strain energy functions for bio-tissue**

Hyperelastic constitutive laws are often employed to model the mechanical response of bio-tissues. Based on experimental data, variety of isotropic and anisotropic strain energy functions have been proposed in recent years. In all these forms of strain energy function, they can be grouped into two categories, in terms of their independent variables. The first group is *the strain-based forms* group, which is expressed directly in terms of the components of suitable strain tensor (often is Green strain tensor $\boldsymbol{E}$ ).The general decoupled form of this group is given below

$$\Psi = \Psi^{dev}(\boldsymbol{E}) + \Psi^{vol}. \tag{11}$$

In the beginning of the development of biomechanics, almost all strain energy functions are formed using Green strain tensor, like Fung's form (Chuong and Fung 1986), "Pole-zero" form (Nash and Hunter 2000), and McCulloch form (Vetter and McCulloch 2000). Although these forms are the naturally transited from elastic constitutive law, they are boring in finding the material parameters and constructing the local material coordinate systems for their needs of an orthogonal coordinate system.

Another group is *the invariant-based forms* group, strain energy functions are expressed in terms of invariants of right Cauchy-Green strain tensor $I_1$, $I_2$ and fiber directions $I_i$ (i=4,5,…), and the general form is given as below

$$\Psi\left(I_1, I_2, J, I_4, ...\right) = \Psi^{dev}\left(I_1, I_2, I_4, ...\right) + \Psi^{vol}\left(J\right), \tag{12}$$

where $J$ is the volume ratio and $J = \sqrt{I_3}$ . Note that in S-FEM, all invariants should use the smoothed version. Material parameters of invariant-based form are less than strain-based form and often just need the fiber orientation. With these advantages, this type is more and more popular in biomechanics, like the recently proposed Holzapfel-Gasser-Odgen (H.G.O) form (Gasser, Ogden, and Holzapfel 2006) for adventitial layers.

There is also a group of strain energy function in terms of *principal stretches*, such as the Ogden form (Ogden 1972). Although they should be categorized in another group for its variables, the principal stretches can be derived form invariants of right Cauchy-Green strain tensor, so we regard they are just special version of the invariant-based forms.

## Numerical examples

*1. Transversely isotropic hyperelastic plate under uniform pressure*

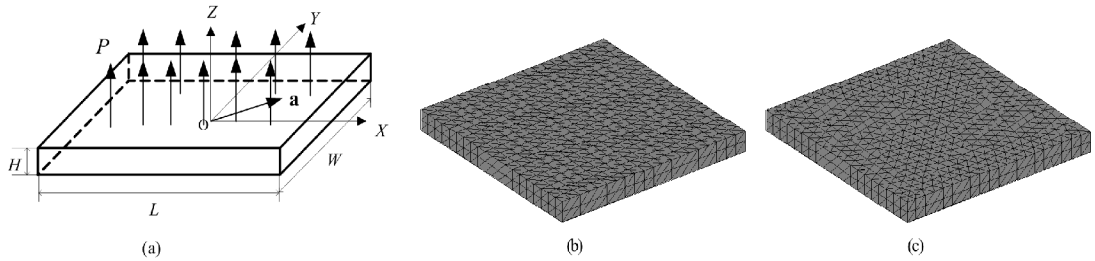


Figure 3. (a) Problems settings of example 3, regular mesh (b) and irregular mesh (c) at initial configuration

The model configuration of one family of fiber-reinforced hyperelastic plate is showed in Figure 3, where L = 1m, W = 1m, H = 0.1m, and $\boldsymbol{a}$ is the unit vector in fiber orientation. The regular mesh and one kind of irregular mesh are plotted in Figure 3(b)(c). Nearly-incompressible Mooney-Rivlin model is employed as the isotropic part of strain energy with the parameters: $C_{10}=1\text{kPa}$, $C_{01}=0.5\text{kPa}$, $\kappa=1000\text{mPa}$ and density $\rho_0=1000\text{kg/m}^3$. Weiss polynomial form (Weiss, Maker, and Govindjee 1996) is employed as deviatoric part of strain energy function with parameter: $A_1=5\text{kPa}$. This strain energy function can be written in following form.

$$\Psi\left(I_1,I_2,J,I_4,...\right)=\Psi_{iso}^{dev}\left(I_1,I_2\right)+\Psi_{ani}^{dev}\left(I_1,I_2,I_4,...\right)+\Psi^{vol}\left(J\right),$$
$$\Psi_{iso}^{dev}\left(I_1,I_2\right)=C_{01}(I_1-3)+C_{10}\left(I_2-3\right),\Psi_{ani}^{dev}\left(I_1,I_2,I_4,I_5\right)=\frac{A_1}{2}\left(I_4-1\right)^2. \tag{13}$$

The boundary condition and initial condition are given as follows. *Initial condition*: $\boldsymbol{v}^0=\boldsymbol{0}$ and $\boldsymbol{u}^0=0$. *Boundary condition*: on the four lateral surface $u_x^n=u_y^n=u_z^n=0$. *Loading*: on the upper surface, a given uniform pressure is applied. This example is aimed to illustrate the ability S-FEM to solve large anisotropic deformation caused by transversely isotropic constitutive law.

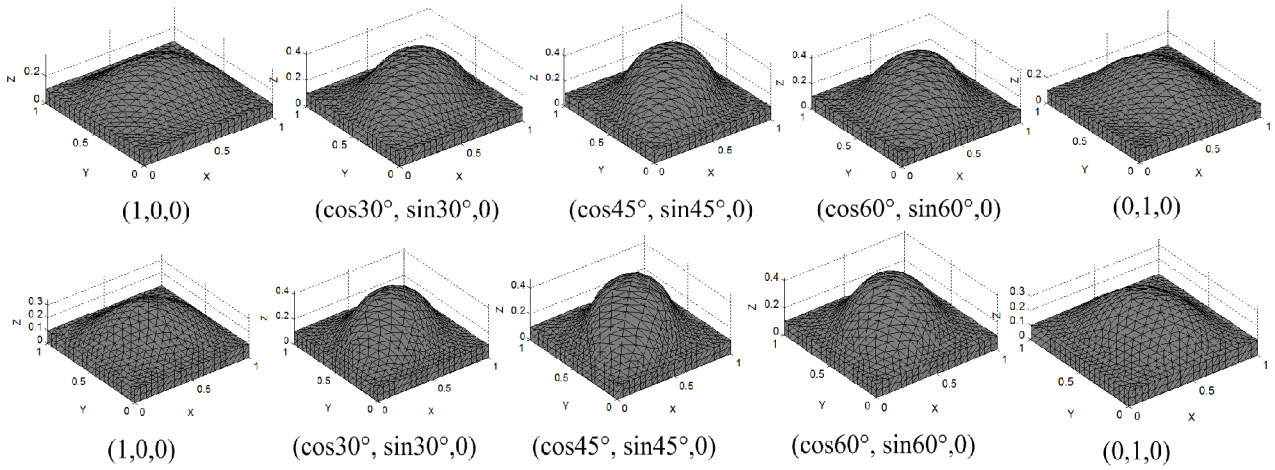


Figure 4. Deformed configurations for regular (above) and irregular meshed (below) example 1 with different fiber directions

Explicit analyses with conventional dynamic relaxation technique are only performed using Selective S-FEM with 7058 TET4 elements (5088 nodes) to achieve the quasi-static solutions. Five different fiber orientations cases are calculated here, and the corresponding orientation vectors

are $(\cos 0^\circ, \sin 0^\circ, 0)$ , $(\cos 30^\circ, \sin 30^\circ, 0)$ , $(\cos 45^\circ, \sin 45^\circ, 0)$ , $(\cos 60^\circ, \sin 60^\circ, 0)$ , and $(\cos 90^\circ, \sin 90^\circ, 0)$. The deformation configurations of different cases are plotted in Figure 4. It is obvious that different embedded fiber direction will lead to a quite different deformation. Moreover, according to definition of transversely isotropic, deformation configurations of cases with fiber direction $(\cos 0^\circ, \sin 0^\circ, 0)$ and $(\cos 90^\circ, \sin 90^\circ, 0)$ should be identical, so as to $(\cos 30^\circ, \sin 30^\circ, 0)$ and $(\cos 60^\circ, \sin 60^\circ, 0)$. For clear demonstration of this phenomenon, displacements of Z-axis in the two upper face diagonal lines are plotted in Figure 5. In Figure 5, nodes with the same distance to the center of plate will have the same deflections in every different fiber direction cases. Also in this figure, results of regular and irregular mesh are matched very well. This example demonstrates that the present selective S-FEM using TET4 is capable to handle the transversely isotropic hyperelastic material in large deformation.

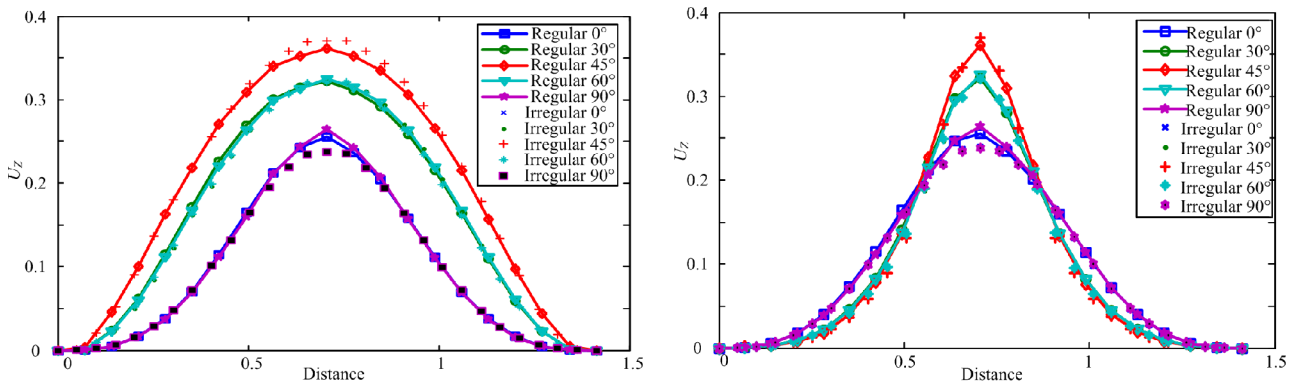


Figure 5. The deflections on the diagonal line (0, 0, 0.1) – (1, 1, 0.1) (left) and (1, 0, 0.1) – (0, 1, 0.1) (right) versus distances to point (0, 0) of regular and irregular meshed cases with different fiber orientations.

*2. Passive filling of rabbit ventricles*

Heart, as the most important organ in any species of animals, pumps blood to other organs and muscles by repeated, rhythmic contractions and expansions. Two phases can be divided in the cardiac cycle; one is the contraction period, referred as *ventricular systole*, another is the *ventricular diastole* which the heart is relaxed and refilled for the next cycle.

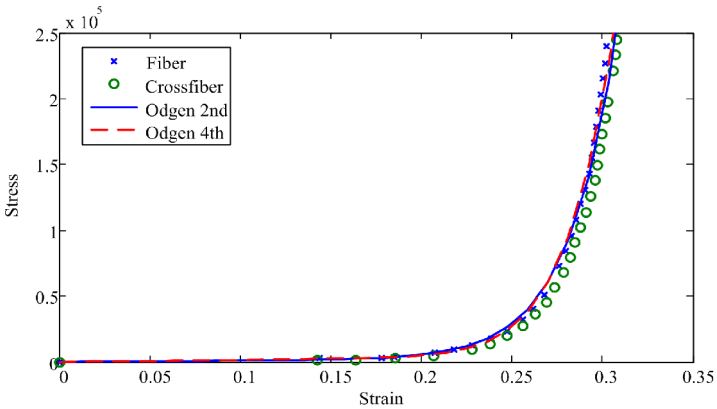


Figure 6. Stress-strain curves of fiber, cross fiber and fitted Ogden forms.

This heart pump depends mainly on the active mechanical property of left ventricle myocardium. Here for the sake of simplicity, the passive filling process is calculated to approximate the *diastole* phase, because of its easier passive mechanical property and loading. Usually, myocardium is fiber-reinforced, and its fibers are complex distributed. According to reference (Lin and Yin 1998) and reference (Vetter and McCulloch 2000), they provide a invariant-based transversely isotropic strain energy function for rabbit myocardium and corresponding equibiaxial stress-strain curves. Luckily, because *the correlation of the fiber and crossfiber strain-stress curves is 0.998631*, anisotropy can be ignored. Ignoring the anisotropy of fiber architecture really can reduce many works on reconstructing the fiber orientations. We fit these two curves into Ogden form strain energy function (Ogden 1972) as in Figure 6. In Figure 6, the

2nd and 4th order Ogden forms can well approximate the curves in the fiber direction and cross fiber direction. For the sake of less parameters, the 2nd Ogden form here is employed as the constitutive law, the decoupled form is

$$\Psi = \sum_{i=1}^{N} \frac{2\mu_i}{\alpha_i^2}\left(\bar{\lambda}_1^{\alpha_i} + \bar{\lambda}_2^{\alpha_i} + \bar{\lambda}_3^{\alpha_i} - 3\right) + \frac{1}{2}\kappa(J-1)^2 \tag{14}$$

where modified principal stretches $\bar{\lambda}_a = J^{-1/3}\lambda_a$ $(a = 1,2,3)$, $N$=2 for 2nd Ogden form, $\mu_i$ (Pa) and $\alpha_i$ are the material coefficients, $\kappa$ is the bulk modulus. Here, for the rabbit myocardium, $\mu_1 = 1803.71\text{Pa}$, $\alpha_1 = -0.924$, $\mu_2 = 5.96\text{Pa}$, $\alpha_2 = -25.0$, and $\kappa = 35590.19\text{Pa}$.

To validate our Selective S-FEM, standard FEM with TET10 elements is employed here to do a comparison. The rabbit ventricle model is discretized by 39142 elements, 9069 nodes for Selective S-FEM, 62239 nodes for FEM, see it in Figure 7 (left). *Boundary condition*: LV and RV endocardial base is constrained the longitude (*X*-direction) displacements, epicardial base are fixed constrained. *Loading*: The 25mmHg pressure is smoothly applied on the LV surface to simulate the passive filling process, and the RV is unloaded here.

A slice of rabbit ventricles in *X*-*Y* plane is drew in Figure 7 (Right) as a simple validation of TET4 Selective S-FEM and TET10 FEM. In Figure 7 (Right), the blue dash curve is the undeformed outline of TET10 FEM slice, the red dot curve is the deformed outline of TET10 FEM slice, but the contour of displacement magnitude belongs to TET4 FS/NS-FEM. The two deformed outline match with each other very well, except some mismatches in the septum. This example shows the near quadratic tetrahedron element accuracy of Selective S-FEM.

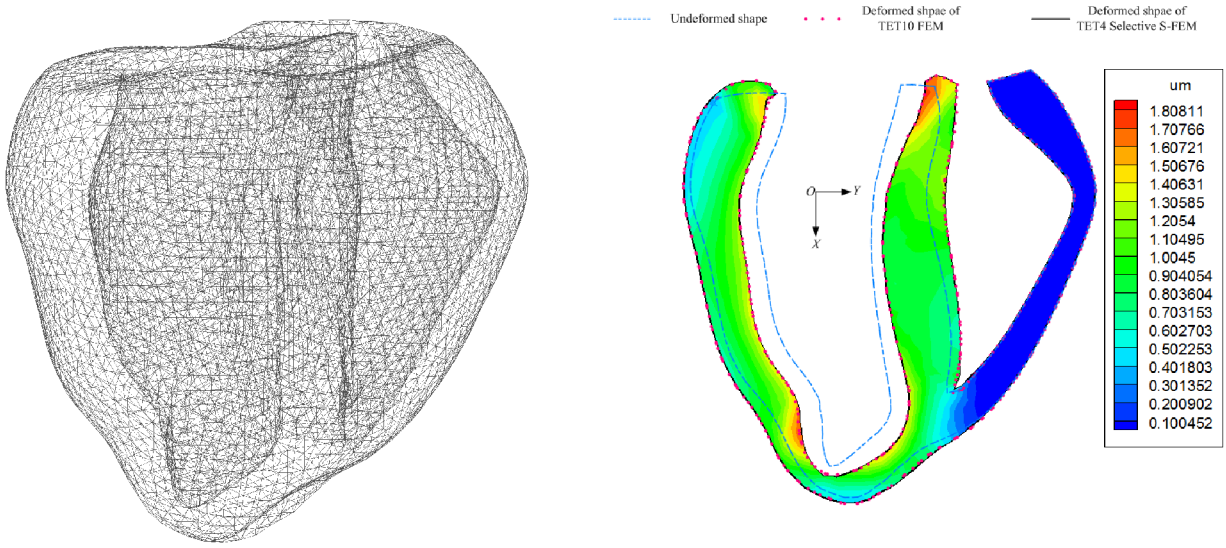


Figure 7. Mesh of rabbit ventricles (left) and a slice in *X*-*Y* plane (right, outline belongs to FEM TET10, contour belongs to FS/NS-FEM).

## Conclusions

In this paper, Selective FS/NS-FEM is applied into isotropic and anisotropic incompressible bio-tissues. Several conclusions can be derived from this paper.

(1) Selective S-FEM using TET4 element can easily mesh complex geometry, such as ventricles.
(2) FS-FEM is ideal for the deviatoric part of deformation of incompressible isotropic or anisotropic solids, so as to greatly improve the performance of the linear elements.

(3) NS-FEM is ideal for the volumetric part of deformation of incompressible solids, and can effectively mitigate the volumetric locking in incompressible materials, even if linear elements are used.
(4) Selective S-FEM is capable to handle the large rotation of fibers in anisotropic bio-tissues with regular or irregular mesh.
(5) Selective S-FEM can enhance the accuracy of linear TET4 element to be closer to quadratic TET10 element.

**Acknowledgments**

This work is partially supported by NSF with Grant No. 1214188 awarded to the senior author, and the A*Star, Singapore to the 2nd author. It is also partially supported by the Open Research Fund Program of the State Key Laboratory of Advanced Technology of Design and Manufacturing for Vehicle Body, Hunan University, P.R.China under the grant number 40915001.

**References**

Belytschko, Ted, W.K Liu, and B. Moran. (2000). *Nonlinear Finite Elements for Continua and Structures*. Wiley.

Bonet, J., and A. J. Burton. (1998). A Simple Average Nodal Pressure Tetrahedral Element for Incompressible and Nearly Incompressible Dynamic Explicit Applications. *Communications in Numerical Methods in Engineering*. 14. (5).pp: 437–449.

Bonet, J., H. Marriott, and O. Hassan. (2001). An Averaged Nodal Deformation Gradient Linear Tetrahedral Element for Large Strain Explicit Dynamic Applications. *Communications in Numerical Methods in Engineering*. 17. (8).pp: 551–561.

Chen, Jiun-Shyan, Sangpil Yoon, and Cheng-Tang Wu. (2002). Non-linear Version of Stabilized Conforming Nodal Integration for Galerkin Mesh-free Methods. *International Journal for Numerical Methods in Engineering*. 53. (12).pp: 2587–2615.

Chuong, C. J., and Y. C. Fung. (1986). On Residual Stresses in Arteries. *Journal of Biomechanical Engineering*. 108. (2).pp: 189.

Gasser, T Christian, Ray W Ogden, and Gerhard a Holzapfel. (2006). Hyperelastic Modelling of Arterial Layers with Distributed Collagen Fibre Orientations. *Journal of the Royal Society, Interface / the Royal Society*. 3. (6).pp: 15–35.

Goudreau, G.L., and J.O. Hallquist. (1982). Recent Developments in Large-scale Finite Element Lagrangian Hydrocode Technology. *Computer Methods in Applied Mechanics and Engineering*. 33. (1-3).pp: 725–757.

Lin, D. H. S., and F. C. P. Yin. (1998). A Multiaxial Constitutive Law for Mammalian Left Ventricular Myocardium in Steady-State Barium Contracture or Tetanus. *Journal of Biomechanical Engineering*. 120. (4).pp: 504.

Liu, G. R. (2009). A G Space Theory and a Weakened Weak (W 2 ) Form for a Unified Formulation of Compatible and Incompatible Methods: Part II Applications to Solid Mechanics Problems. *International Journal for Numerical Methods in Engineering*.pp: n/a–n/a.

Liu, G. R., K. Y. Dai, and T. T. Nguyen. (2006). A Smoothed Finite Element Method for Mechanics Problems. *Computational Mechanics*. 39. (6).pp: 859–877.

Liu, G. R., and G. Y. Zhang. (2009). A Normed G Space and Weakened Formulation of a Cell-based Smoothed Point Interpolation Method. *International Journal of Computational Methods*. 06. (01).pp: 147–179.

Liu, G.R., T. Nguyen-Thoi, and K.Y. Lam. (2009). An Edge-based Smoothed Finite Element Method (ES-FEM) for Static, Free and Forced Vibration Analyses of Solids. *Journal of Sound and Vibration*. 320. (4-5).pp: 1100–1130.

Liu, G.R., and G.Y. Zhang. (2013). *The Smoothed Point Interpolation Methods – G Space Theory and Weakened Weak Forms*. WorldScientific.

Miller, Karol, Grand Joldes, Dane Lance, and Adam Wittek. (2006). Total Lagrangian Explicit Dynamics Finite Element Algorithm for Computing Soft Tissue Deformation. *Communications in Numerical Methods in Engineering*. 23. (2).pp: 121–134.

Nash, M P, and P J Hunter. (2000). Computational Mechanics of the Heart. *October*. 61. (1).pp: 113–141.

Nguyen-Thoi, T., G. R. Liu, K. Y. Lam, and G. Y. Zhang. (2009). A Face-based Smoothed Finite Element Method (FS-FEM) for 3D Linear and Geometrically Non-linear Solid Mechanics Problems Using 4-node Tetrahedral Elements. *International Journal for Numerical Methods in Engineering*. 78. (3).pp: 324–353.

Nguyen-Thoi, T., H.C. Vu-Do, T. Rabczuk, and H. Nguyen-Xuan. (2010). A Node-based Smoothed Finite Element Method (NS-FEM) for Upper Bound Solution to Visco-elastoplastic Analyses of Solids Using Triangular and Tetrahedral Meshes. *Computer Methods in Applied Mechanics and Engineering*. 199. (45-48).pp: 3005–3027.

Ogden, R. W. (1972). Large Deformation Isotropic Elasticity - On the Correlation of Theory and Experiment for Incompressible Rubberlike Solids. *Proceedings of the Royal Society A: Mathematical, Physical and Engineering Sciences*. 326. (1567).pp: 565–584.

De Souza Neto, E.A., D. Perić, M. Dutko, and D.R.J. Owen. (1996). Design of Simple Low Order Finite Elements for Large Strain Analysis of Nearly Incompressible Solids. *International Journal of Solids and Structures*. 33. (20-22).pp: 3277–3296.

Taylor, Robert L. (2000). A Mixed-enhanced Formulation Tetrahedral Finite Elements. *International Journal for Numerical Methods in Engineering*. 47. (1-3).pp: 205–227.

Vetter, FJ, and AD McCulloch. (2000). Three-dimensional Stress and Strain in Passive Rabbit Left Ventricle: a Model Study. *Annals of Biomedical Engineering*. 28.pp: 781–792.

Weiss, Jeffrey A., Bradley N. Maker, and Sanjay Govindjee. (1996). Finite Element Implementation of Incompressible, Transversely Isotropic Hyperelasticity. *Computer Methods in Applied Mechanics and Engineering*. 135. (1-2).pp: 107–128.

Zienkiewicz, O. C., J. Rojek, R. L. Taylor, and M. Pastor. (1998). Triangles and Tetrahedra in Explicit Dynamic Codes for Solids. *International Journal for Numerical Methods in Engineering*. 43. (3).pp: 565–583.